Dynamic Calibration and Occlusion Handling Algorithms for Lane Tracking

Bing-Fei Wu, *Senior Member, IEEE*, Chuan-Tsai Lin, *Student Member, IEEE*, and Yen-Lin Chen, *Member, IEEE*

***Abstract*—An approach of rapidly computing the projective width of lanes is presented to predict the projective positions and widths of lanes. The Lane Marking Extraction Finite State Machine is designed to extract points with features of lane markings in the image, and a cubic B-spline is adopted to conduct curve fitting to reconstruct road geometry. A statistical search algorithm is also proposed to correctly and adaptively determine thresholds under various kinds of illumination conditions. Furthermore, the parameters of the camera in a moving car may change with the vibration, so a dynamic calibration algorithm is applied to calibrate camera parameters and lane widths with the information of lane projection. Moreover, a fuzzy logic is applied to determine the situation of occlusion. Finally, a region-of-interest determination strategy is developed to reduce the search region and to make the detection more robust with respect to the occlusion on the lane markings or complicated changes of curves and road boundaries.**

***Index Terms*—Autonomous vehicle, driving assistance, fuzzy logic, lane detection, vision-based.**

I. Introduction

IN THE DRIVING assistant systems, traffic information can be acquired by sensors to make driving safe and easy [1], [2]. For example, vision-based driving assistant systems can determine positions of lanes and obstacles preceding a host vehicle, and the detected information can serve as guidance for driving safety of vehicles [3]–[5]. In the system, the detection of lane is based on image processing techniques to search for the road edges or the lane markings [6], [7], and then, the lane information is applied to the detection of obstacles in determining obstacle positions [8]–[10]. However, occlusions of obstacles on lane markings may affect results of lane detection [11]. Therefore, lane detection requires not only fast executive speed to achieve real-time detection but also a solution to occlusions.

There are many ways that lane detection can be achieved. In early studies, Dickmanns and Mysliwetz [12] conducted a 3-D road recognition by adopting horizontal and vertical mapping models, the approach of extracting features with edge elements, and recursive estimation techniques. The results were applied to their test vehicle (VaMoRs) to function as autonomous vehicle guidance. Broggi *et al.* [13], [14] used inverse perspective mapping (IPM) to transfer a 3-D world coordinate to a 2-D image coordinate and detected road markings using top-view images. Kreucher and Lakshmanan [15] suggested detecting lane markings with frequency-domain features that capture relevant information about edge-oriented features. The objectives of many studies on lane detection include autonomous vehicle guidance and driving assistance such as lane-departure-warning and driver-attention monitoring systems. Some assumptions in common are as follows: 1) The road is flat or follows a precise model; 2) the appearance of lane markings follows strict rules; and 3) the road texture is consistent. The main difficulty in lane detection is how to recognize roads efficiently in various situations, including complex shadowing and changes in illumination [8], [16]. Furthermore, the vibration of a moving camera causes changes in camera parameters and thus leads to errors in geometric transformation. To solve the problem, dynamic calibration of cameras is required to improve robustness [17]–[22].

The task of lane detection can be summarized as two main sections: 1) the acquisition of features and 2) a road model for reconstructing road geometry. In addition, to accelerate the detection and make it robust, some approaches are added such as narrowing the search region, the determination of region of interest (ROI), dynamic calibration for the camera, and position-tracking methods using consecutive images.

The first step of detecting lanes is to extract their features. On most occasions, there are lane markings on both the left and the right side of the driving lane, while, sometimes, only the boundaries of the road exist without any lane marking. Most parts of the lane markings are like two parallel ribbons with some variations, for example, being straight or curved, solid lines or dashed lines, and in the color of white, yellow, or red. The occlusion of trees and buildings and their shadows makes it more difficult to detect positions of lanes. In addition, visibility varying with illumination adds difficulty to detections [7], [23].

In acquiring features, there are four major types of methods: pixel-based, edge-detection-based, marking-based, and color-based methods. The pixel-based type is to classify pixels into certain domains and to put pixels of the road boundaries in one category [24]–[26]. The edge-detection-based type involves conducting edge detection in the image first. Then, find straight lines with Hough transform [27], [28] or adopt an ant-based approach to start a bottom–up search for possible path of the road boundary in the image [29]–[32] or determine search regions by road models for detection of road boundaries

Manuscript received January 30, 2008; revised November 11, 2008. First published January 6, 2009; current version published April 29, 2009. This work was supported by the National Science Council of Taiwan under Grant NSC97-2752-E-009-012–PAE and Grant NSC-96-2218-E-468-006.

B.-F. Wu and C.-T. Lin are with the Department of Electrical and Control Engineering, National Chiao Tung University, Hsinchu 30050, Taiwan (e-mail: bwu@cssp.cn.nctu.edu.tw; chuantsai@cssp.cn.nctu.edu.tw).

Y.-L. Chen is with the Department of Computer Science and Information Engineering, Asia University, Taichung 41354, Taiwan (e-mail: ylchen@cssp.cn.nctu.edu.tw).

Color versions of one or more of the figures in this paper are available online at http://ieeexplore.ieee.org.

Digital Object Identifier 10.1109/TIE.2008.2011295

[33]–[36]. Those two methods are time-consuming and easily cause errors when complex shadows or obstacle occlusion exists. The marking-based type is based on features of lane markings. For example, Bertozzi and Broggi [14] proposed IPM and black–white–black transitions to detect lane markings. This method may effectively deal with some situations of shadows or obstacle occlusions. However, the vibration caused by the moving vehicle may influence the extrinsic parameters of the camera and thus arouse unexpected mapping distortions on images, which may cause errors on lane detection results. The color-based type is to utilize color information of the road in the image [26], [37]–[39]. In this way, there is more information about the lane and better abilities to resist noise. However, it takes more computation time to extract color features of interest.

Since shadows of trees or other noises usually exist and some lane markings are dash lines, the detected features of road boundaries are often incomplete. Therefore, the methods of interpolation or curve fitting are needed to reconstruct the road geometry. Kreucher and Lakshmanan [15] used a deformable template shape model to detect lanes. They believed that two sides of a road respectively approximate a quadratic equation, so they established their coefficients to determine the curvature and orientation of the road. However, curve fitting cannot be done by a quadratic equation on the lanes with S-shaped turns. Therefore, Wang *et al.* [40] adopted spline interpolation which can be used in various curves to connect line segments. However, when there are vehicles in the lane occluding parts of the lane boundary, some errors may arise, because this approach found a vanishing point depending on Hough transform followed by line-length voting. Thus, vehicles on the lanes may form spurious lines which may influence the determination of the vanishing line. Furthermore, Hough transform and Canny edge detector utilized in the approaches of Wang *et al.* may take more computation time.

Another issue to promote lane detection efficiency and depress noise sensitivity is to set appropriate ROI. Lin *et al.* [41] applied the information of both lane boundaries obtained from initial detection in the first frame to the finding of ROI on Hough domain. Then, ROI was adopted as search parameters of lane boundaries in the subsequent frames. The method can effectively accelerate lane detection process on a straight lane, but errors may arise on road curves. The method of Chapuis *et al.* [6] utilized an initially determined ROI to recursively recognize a probabilistic model to conduct iterative computation and adopted a training phase to define the best interesting zone. The initially set ROI is effective in the general roads; however, diverse road curves may make the initial ROI too large on the farther part of the road and thus raise noise sensitivity. Therefore, an effective method is needed for adaptive determination of ROI and adjustment to changes of road curves in the image sequences, and thus, ROI can be significantly narrowed to obtain more accurate and faster lane detection results.

This paper applied geometry transformation and a method of rapid computation of lane width to predict the projective positions and widths of lanes and markings. Then, an approach named the Lane Marking Extraction (LME) Finite State Machine (FSM) is designed to find lane markings efficiently. A statistical search algorithm is also proposed to correctly and adaptively determine thresholds under various illumination conditions. Furthermore, a dynamic calibration algorithm is presented to update the information of a camera's parameters and lane widths. Moreover, a fuzzy logic scheme is adopted to judge the correctness of the detected lane markings, and the results are applied to the selection of knots when reconstructing road geometry by B-spline. Finally, the ROI determination strategy is proposed to constrain the search region to make the detection more robust and fast. Therefore, even though obstacles occlude parts of the lane markings, road boundaries can still be reconstructed correctly. Moreover, the relative positions between lane markings and cameras can be more precisely estimated with the camera tilt obtained through dynamic calibration.

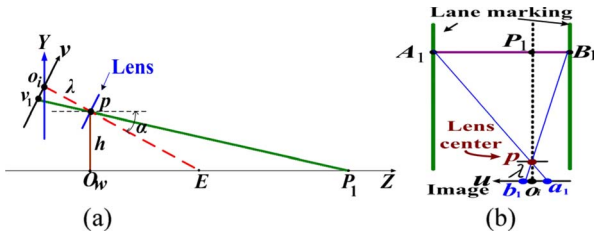

Fig. 1. Projective geometry of a camera model. (a) The mapping of the Y- and Z-coordinates on the v-coordinate. (b) The mapping of the X- and Z-coordinates on the u-coordinate.

This paper is organized as follows. Section II presents image analyses using a camera model and the approach of dynamic calibration. Section III describes the proposed approaches to lane detection, including analyses of lane features, a novel LME method adopting an FSM, a strategy for determining ROI, postprocessing by fuzzy reasoning, the determination of road boundaries by B-spline curve fitting, and overall process of lane detection. Then, the experimental results of lane detection and analyses are shown in Section IV. Section V concludes the paper.

II. Camera Model With Dynamic Calibration

The position of any point in the 3-D world coordinates (X, Y, Z) projected onto a 2-D image plane (u, v) can be obtained through perspective transformation [23]. According to an assumption of a flat ground, mapping a point of the ground plane onto an image plane is a one-to-one transformation. This transformation of the two coordinates can be employed to estimate the distance between the camera and any point on the ground.

A. Camera Model

In our previous work [7], a simple camera model was presented to estimate lane projection. In this paper, this camera model is extended. Based on this new model, some techniques have been developed. Fig. 1 shows the projective geometry of a camera model, where O_w denotes the origin of the world coordinates (X, Y, Z) and O_i represents the origin of the image coordinates (u, v, w). Let λ, p, and h be the focal length of

the camera, the lens center, and the height between p and O_w, respectively, so $(0, h, 0)$ would be the lens center in the world coordinate.

In Fig. 1(a), the parameter α is the tilt angle, representing the angle between the Z-axis and the optical axis, $\overline{O_i E}$. In Fig. 1(a), a point in $P_1(X, 0, Z)$ in the world coordinates is mapped onto $v_1(u, v)$ in the image coordinates. The relation between Z and v is shown as (1), and the vertical distance between P_1 and the camera is $\overline{O_w Z}$, where

$$Z = h \cdot \tan\left(\left(\frac{\pi}{2} - \alpha\right) - \tan^{-1}\left(\frac{v}{\lambda}\right)\right). \tag{1}$$

Fig. 1(b) is a top view of the actual lane. As illustrated, $A_1(X_1, 0, Z)$ is a point on the left lane marking and $B_1(X_2, 0, Z)$ is a point on the right one. With the known Z-coordinate obtained from (1), the X-coordinate determines where in the u-coordinate A_1 and B_1 are projected onto. In Fig. 1(b), the lane width is $\overline{A_1 B_1}$ and the width of its projection in the image is $\overline{a_1 b_1}$. Based on similar triangles, the relation between $\overline{a_1 b_1}$ and $\overline{A_1 B_1}$ is shown as

$$\overline{a_1 b_1} = \overline{A_1 B_1} \times \lambda / Z. \tag{2}$$

According to (1) and (2), the projective lane width can be appropriately predicted and can be applied to the following lane detection process. Similarly, the projective width of lane markings can also be correctly estimated.

B. Rapid Estimation of the Projective Width

With the known lane width on the world coordinate, the corresponding projective width of the lane can be computed by (1) and (2). However, the computation of trigonometric functions is time-consuming. In this paper, an approach for rapid estimation of projective lane width is proposed, in which W_{WL} represents the width of a lane in the world coordinates, and its associated width of lane projection in the v-coordinate is $w_L(v)$. The relation between $w_L(v)$ and the v-coordinate can be expressed by a linear equation as shown in (3). The approach can suppress the computation cost of trigonometric functions. The proof is presented in Appendix A

$$w_L(v) \doteq \left(\frac{W_{WL}}{h}\right) \times v + c \tag{3}$$

where c is a translation.

In Fig. 2, take the internal parameters of the Hitachi KP-F3 camera for example. The relation between $w_L(v)$ and the v-coordinate is computed by (2) and (3). The physical pixel size is 7.4 μm(H) $\times$ 7.4 μm(V), and the focal length $\lambda = 15$ mm. The height h is 1.32 m, and the lane width is set to be 3.3 m. The horizontal axis represents the v-coordinate of the lane projection, while the vertical stands for the projective width. Line (W_A) shows the estimation result of projective lane width when $\alpha = 3°$, and Line (W_B) demonstrates the result when $\alpha = 10°$. As shown in Fig. 2, with a fixed parameter of the camera, the relation between $w_L(v)$ and the v-coordinate is

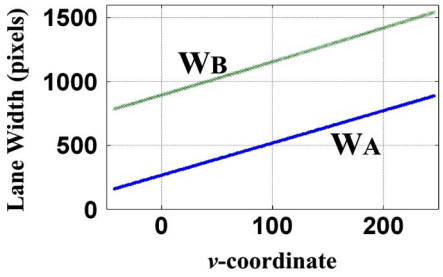

Fig. 2. Relation between $w_L(v)$ and the v-coordinate.

linear. To estimate c in (3), let the projective lane width be w_1, when it is projected onto v_1. w_1 is obtained from the computation of (1) and (2). Substitute v_1 and w_1 for v and $w_L(v)$ in (3), respectively, and c is derived from (4). Therefore, the relation between w_L and the v-coordinate can be depicted in (5). Take two points on the line from the slope in Fig. 2, and the slope is computed as 2.51. Compared with the slope $W_{WL}/h = 2.5$ in (3), these two results are very similar. Therefore, the calculation of (2) and (3) can be replaced with the approach of rapid computation of the width to reduce computation cost

$$c = w_1 - \left(\frac{W_{WL}}{h}\right) \times v_1 \tag{4}$$

$$w_L = \left(\frac{W_{WL}}{h}\right) \times v + w_1 - \left(\frac{W_{WL}}{h}\right) \times v_1. \tag{5}$$

Likewise, the projective width of the lane markings w_m can be shown by

$$w_m(v) \doteq \left(\frac{W_{wm}}{h}\right) \times v + c_1 \tag{6}$$

where W_{wm} denotes the actual width of lane markings and c_1 is a translation.

C. Dynamic Calibration

In computing lane width with coordinate transformation, if the tilt angle of the camera is not accurate, huge errors may arise [19]. However, even though the preset tilt angle of the camera is known, there are still some errors because of the road bumps and vibration of moving vehicles. In this paper, an accurate tilt angle and actual lane width can be obtained by using the extracted lane markings in each frame.

1) Calibration of the Tilt Angle of Camera: In this paper, lane markings are supposed to be two parallel lines, and thus, their intersection Z_i would be at infinity. In the image, the intersection of the extension of the two lane markings is the vanishing point $V_P(u_{vp}, v_{vp})$, with mappings onto Z_i. According to (1), the relation of α, Z_i, and v_{vp} is shown as (7). Substitute (8) into (7), and α is shown as (9). Therefore, α can be obtained through V_P. Furthermore, let the four points of the Z-coordinate $= Z_{N1}$, and Z_{N2} on the left and right lane markings, i.e., Q_{L1}, Q_{L2}, Q_{R1}, Q_{R2}, respectively, mapping onto P_{L1}, P_{L2}, P_{R1}, and P_{R2} in the image plane. As shown in Fig. 3, suppose that the lane width is fixed, $\overline{Q_{L1} Q_{R1}} =$

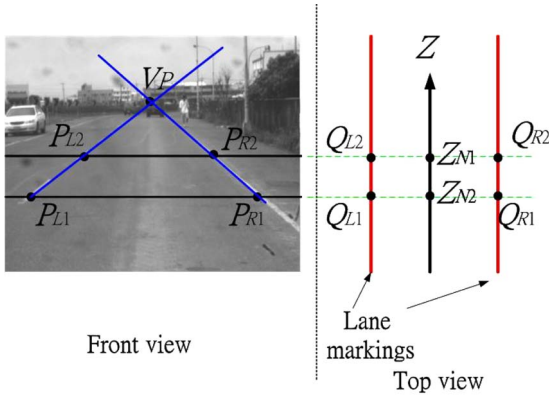

Fig. 3. Estimated vanishing point.

$\overline{Q_{L2}Q_{R2}}$, and the area enclosed by the closed area formed by the four points will be a parallelogram in the world coordinate. Extend $\overline{P_{L1}P_{L2}}$ and $\overline{P_{R1}P_{R2}}$, and the intersection of them is also a vanishing point, V_P. Then, v_{vp} is derived from (10). In this paper, V_P is determined this way to avoid the wrong calculation caused by the blur or occlusion in the farther part of the lane marking

$$\alpha = \pi/2 - \tan^{-1}(v_{vp}/\lambda) - \tan^{-1}(Z_i/h) \tag{7}$$

$$\lim_{Z_i \to \infty} \tan^{-1}(Z_i/h) = \pi/2 \tag{8}$$

$$\alpha = -\tan^{-1}(v_{vp}/\lambda) \tag{9}$$

$$v_{vp} = \frac{f_2}{f_1}$$

$$f_1 = \frac{v_{R1} - v_{R2}}{u_{R1} - u_{R2}} - \frac{v_{L1} - v_{L2}}{u_{L1} - u_{L2}}$$

$$f_2 = \left(\frac{u_{L1}v_{L2} - v_{L1}u_{L2}}{u_{L1} - u_{L2}}\right)\left(\frac{v_{R1} - v_{R2}}{u_{R1} - u_{R2}}\right) - \left(\frac{v_{L1} - v_{L2}}{u_{L1} - u_{L2}}\right)\left(\frac{u_{R1}v_{R2} - v_{R1}u_{R2}}{u_{R1} - u_{R2}}\right) \tag{10}$$

where the coordinates of P_{L1}, P_{L2}, P_{R1}, and P_{R2} are (u_{L1}, v_{L1}), (u_{L2}, v_{L2}), (u_{R1}, v_{R1}), and (u_{R2}, v_{R2}), respectively.

2) Lane Width Refinement: According to the coordinates of P_{L1} and P_{R1}, the associated projective lane width is $|u_{R1} - u_{L1}|$, when projected onto the row at v_{L1}. Substitute $|u_{R1} - u_{L1}|$ and v_{L1} into (1) and (2), and then, the lane width in the world coordinates $\overline{A_1B_1}$ can be estimated. It shows that the lane width can be obtained depending on the detected lane markings. Likewise, the actual width of lane markings can be acquired by applying the width of detected lane markings. Thus, those widths can be accurately gained even when they vary with changes of the environment.

III. Lane Detection

Both sides of road markings are supposed to be parallel on the ground plane, and their widths are assumed to stay stable or have very slight changes. An approach of extracting lane markings based on a lane model is presented in this section.

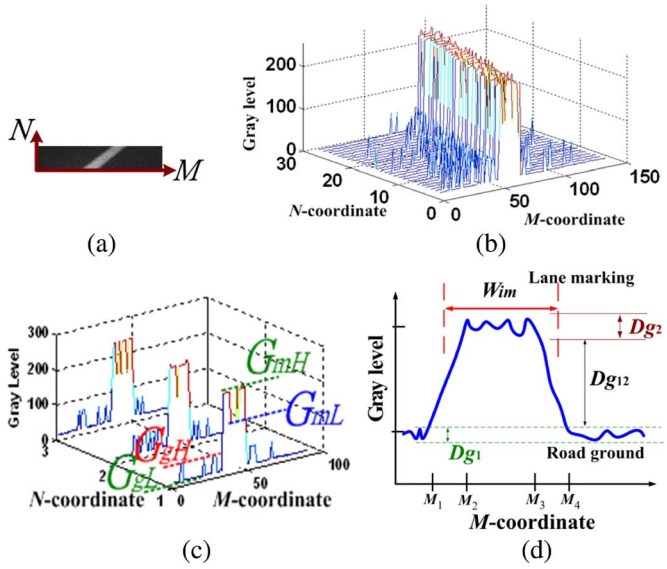

Fig. 4. Lane marking model on a road with lane markings. (a) Actual lane marking image. (b) The gray-level distribution of (a). (c) The gray-level distribution of lane markings in the image coordinates. (d) The variance of gray level in a row of lane marking.

A. Model of Lane Markings

Lane markings usually appear as white, yellow, or red curves and lines. Their intensity in the image is usually higher than that of the ground because they reflect more brightness than road colors. Fig. 4 shows the analysis of a lane marking model. Fig. 4(a) shows a segment of one lane marking. The M-coordinate and the N-coordinate denote the horizontal and vertical coordinates, respectively. Fig. 4(b) shows the gray-level distribution of the pixels in Fig. 4(a). In these figures, it can be observed that the gray level of the lane marking is much higher than that of the ground. Fig. 4(c) shows both the gray-level ranges of lane markings and ground in the image coordinates. As can be seen, G_{mH} and G_{mL}, respectively, denote the lane marking's largest and smallest gray levels, while G_{gH} and G_{gL}, respectively, represent the largest and smallest of the ground's gray levels. Fig. 4(d) shows the gradient model of the gray level in each row of the lane marking, where D_{g1} is the range of ground's gray level. D_{g2} is the range of lane markings' gray level. D_{g12} is the difference between G_{mL} and G_{gH}. A statistical search algorithm is proposed to adaptively determine D_{g1}, D_{g2}, and D_{g12}. They are adaptively adjusted under various illumination conditions. D_{g1}, D_{g2}, and D_{g12} can be determined by (11), and the detailed explanation is given in Appendix B. The zone between M_1 and M_2 is the left border of the lane named BS with an upward trend of the gray level, while the zone between M_3 and M_4 is the right border called BT whose gray levels decline. These features of lane markings are called bright feature transition (BFT). The distance between BS and BT represents the length of BFT and is named by B_L. A lane marking can be reconstructed by searching the BFT row by row and connecting BFTs in each row

$$\begin{aligned} D_{g1} &= G_{gH} - G_{gL} \\ D_{g2} &= G_{mH} - G_{mL} \\ D_{g12} &= G_{mL} - G_{gH}. \end{aligned} \tag{11}$$

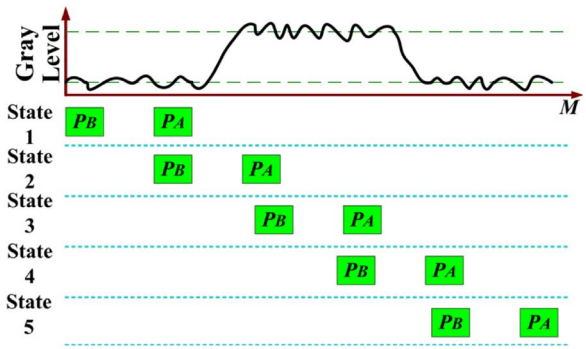

Fig. 5. Lane marking's relative positions to P_A and P_B in different states.

B. Lane Marking Extraction

In the image, the BFT approximates to the width of the lane markings and is possibly part of the lane markings. In this section, an LME FSM is proposed to extract BFT similar to the lane marking width in the images. First, set a BFT detector in each row of the image, which contains two detection points P_A and P_B. The distance between these two points is d_m, as shown in (12). When this BFT detector moves from the left to the right, the difference of the gray levels between P_A and P_B, named $G_d(P_A, P_B)$, will be updated with respect to the detector's move to the right. When the BFT detector moves one pixel rightward, $G_d(P_A, P_B)$ is accordingly updated and served as a new input signal of the LME FSM. If bright features are found within the current range of the BFT detector where P_A and P_B are moving, the input of $G_d(P_A, P_B)$ would accordingly transfer the state of LME FSM from State 0 to State 5. Therefore, bright features in every row can be detected according to the transitions of the processing state. If its B_L approximates to the computed width of the lane marking w_m obtained from (6), then the likelihood of its being an actual lane marking is high

$$d_m(N) = \frac{1}{2} \times w_m(N) \tag{12}$$

where $w_m(N)$ denotes the projective width of the lane marking in the N-coordinate. $d_m(N)$ represents the distance between P_A and P_B in the Nth row. The distance is set to be half of the estimated width of the lane marking w_m in the same row. When BFT detector is applied to detect lane markings, the associated change of $G_d(P_A, P_B)$ passing the lane markings can be shown as in Fig. 5.

In Fig. 5, when lane markings appear in the image, the range of $G_d(P_A, P_B)$ will change by five states, associated with BFT detector shifting rightward across a lane marking. In State 1, the interval where the detector is located is a lowland zone. In State 2, the part where the detector lies in is an uphill zone. In State 3, the section with the detector is a plateau zone. In State 4, the detector is in a downhill zone. In State 5, the detector comes back to the lowland zone. Table I shows the range of predictive G_d in those states. If $G_d(P_A, P_B) = G_{d1}$, $G_d(P_A, P_B)$ can match the G_d condition $|G_d| < D_{g1}$. Likewise, the G_d condition of G_{d2}, G_{d3}, and G_{d4} can be obtained from Table I in the same way. Fig. 6 shows the state diagram. The transitional operations of the five states are described as follows.

TABLE I
DENOTATIONS OF THE FIVE G_d CONDITIONS

State	Denotations in different G_d Conditions	G_d Conditions
State 1	G_{d1}	$\|G_d\|<D_{g1}$
State 2	G_{d2}	$G_d>D_{g12}$
State 3	G_{d3}	$\|G_d\|<D_{g2}$
State 4	G_{d4}	$-G_d>D_{g12}$
State 5	G_{d1}	$\|G_d\|<D_{g1}$

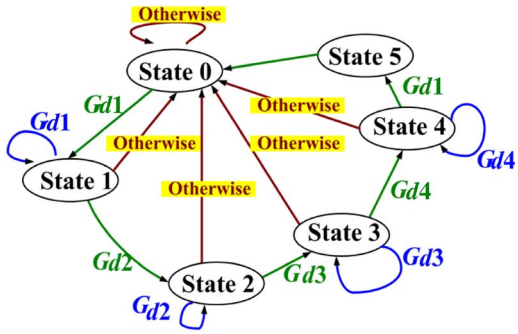

Fig. 6. State diagram of LME FSM.

In State 0, LME FSM is in the initial state, and no bright feature has been detected yet in this state. When $G_d(P_A, P_B)$ satisfies the condition G_{d1}, BFT is possibly within the search region and FSM moves into State 1.

In State 1, the BFT detector lies in the lowland zone. If $G_d(P_A, P_B)$ still meets G_{d1}, then the next state will still be State 1; if $G_d(P_A, P_B)$ satisfies G_{d2}, FSM will move into State 2. Otherwise, FSM goes back to State 0.

In State 2, the BFT detector is located in the uphill zone. If $G_d(P_A, P_B)$ meets G_{d2}, the next state will still be State 2; if $G_d(P_A, P_B)$ meets G_{d3}, FSM will move into State 3. Otherwise, FSM goes back to State 0. As soon as FSM enters State 2, P_A may shift to the region between M_1 and M_2 as in Fig. 4(d), the left border between the lane marking and the gray ground. In this condition, the gray level of P_A would be larger than that of P_B.

In State 3, the BFT detector is in the plateau zone. If $G_d(P_A, P_B)$ meets G_{d3}, the next state is still State 3; if $G_d(P_A, P_B)$ meets G_{d4}, FSM will move into State 4. Otherwise, FSM goes back to State 0. When FSM enters State 3, the BFT detector may have already shifted to the range between M_2 and M_3 as in Fig. 4(d). Now, the gray level of P_A is similar to that of P_B.

In State 4, the BFT detector is situated in the downhill zone. If $G_d(P_A, P_B)$ meets G_{d4}, next state is State 4; if $G_d(P_A, P_B)$ meets G_{d1}, FSM moves into State 5. Otherwise, FSM goes back to State 0. When FSM moves into State 4, P_A may have shifted to the zone between M_3 and M_4 as in Fig. 4(d), the right border between the lane marking and the road ground. Then, the gray level of P_A is smaller than that of P_B.

In State 5, the BFT detector returns to the lowland zone. If FSM enters State 5, that means BFT has been detected and FSM will go back to State 0 to find the next BFT.

LME FSM is efficient in detecting BFT and computing B_L. It is also suitable for hardware implementation.

C. ROI Determination Strategy

In this section, two properties of changes about positions of lane boundaries are introduced. 1) Longitudinal consistency property: From the nearby position to the farther position, lane markings appear to be lines or curves which are either continuous or dashed. Therefore, by observing the positions of the closer lane markings, the possible positions of the farther parts can be accordingly predicted. 2) Lateral consistency property: Vehicles often move in the middle of the lane, so lateral changes of a lane marking's position are usually slight in the sequential road-scene images. Thus, the possible position of the lane marking in the next frame can be predicted according to that of the current one. The predictive area of the lane marking is the ROI, also the search area of BFT. If the ROI is too large, the computation cost would increase and the ROI may be stained by noise. On the other hand, if the ROI is too small, the actual position of the lane marking may not be appropriately covered. Therefore, the ROI should be the smallest area which can still include the area of the lane markings. Strategies for determining the ROI and three determination approaches to the ROI are presented in the subsection. Choosing the best strategy for the associated case is an effective way to reduce errors and computation costs

$$Roi(M, N_p) = \{I(M, N) | M \in [M_L, M_R];\ N = N_p\}. \quad (13)$$

The ROI is illustrated as (13), where $I(M, N)$ represents the image coordinates. The M-coordinate and the N-coordinate, respectively, denote the horizontal and vertical coordinates. Here, the left bottom coordinate is defined as the origin shown in Fig. 8. The ROI in the N_pth row is denoted by $Roi(M_p, N_p)$, where $M \in [M_L, M_R]$, with M_L being the left border within the range and M_R being the right border. Our proposed lane detection method consists of two modes. 1) Single mode: Only the information of the current processed frame is considered. 2) Sequential mode: Using the temporal information of the previous frames to shrink the search area of the current frame so as to accelerate the detection and reduce errors. The selection of the suitable ROI determining strategies for different models is given as follows.

1) In every row, the sequence of ROI is determined by following the bottom–up direction on the N-coordinate and starting from $N = 0$ row to the preset terminal row N_e.
2) In *single mode*, the *fixed area approach*, as depicted in Section III-C1, is first applied to determine the front parts of two lane markings, and then, the coordinates of the detected lane markings are considered the start coordinates of the left and right lane markings. Afterward, the ROI of the farther parts of lane markings is determined by the *expansion approach* to follow the bottom–up direction on N-coordinate to the terminal N_e, as described in Section III-C2.
3) In *sequential mode*, the ROI is determined by the *tracking approach* as described in Section III-C3. If the information of the previous frames does not include N_e, then the *expansion approach* will be conducted to continue the detection to reach N_e.

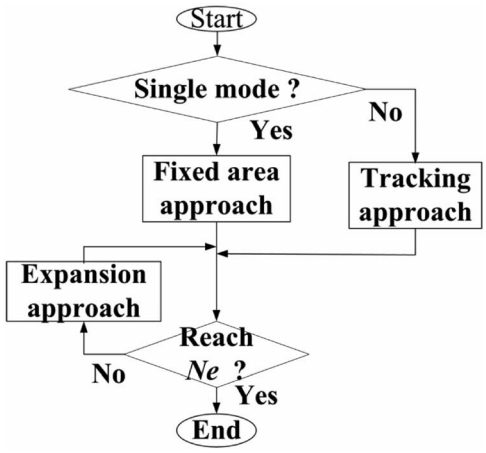

Fig. 7. Flowchart of the selection of ROI determination strategies.

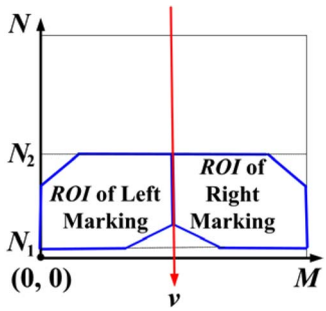

Fig. 8. ROI of fixed area.

The flowchart of selecting ROI determination strategies is shown in Fig. 7.

The following sections will present three kinds of ROI decision approaches.

1) Fixed Area Approach: This approach is to detect the position of the nearby part of the lane marking. As shown in Fig. 8, the determination of the coordinates N_1 and N_2 was based on their mappings onto the two Z-coordinates, respectively, 8 and 25 m on the ground plane because lane markings in this range are usually very clear. After determining N_1 and N_2, let the two hexagonal areas be the ROI, and these sections are divided by the v-axis. The BFTs detected on the left side are the possible positions of the left lane markings, and the ones on the right side are the possible right lane markings. The search area of this approach is larger, and it is used when no temporal information of lane markings is available.

2) Expansion Approach: This approach includes two phases. Phase 1 is a bidirectional expansion scheme. In this scheme, the latest detected position of the BFT is considered as a center, and then, the ROI is determined by expanding row by row along the direction of the N-coordinate, as shown in (14) and (15). Fig. 9(a) shows the ROI set in this way, where the ROI is the area within the two blue dotted lines along the two sides of the lane markings. In this way, the ROI is set by linear equations as in (14) and (15). The approach is simple and rapid, but the ROI may expand when the distance between the current row and the last row is extended. Phase 2 is a tendency expansion scheme. This approach is performed by computing the slope of the lane marking to predict its trend and expanding along the

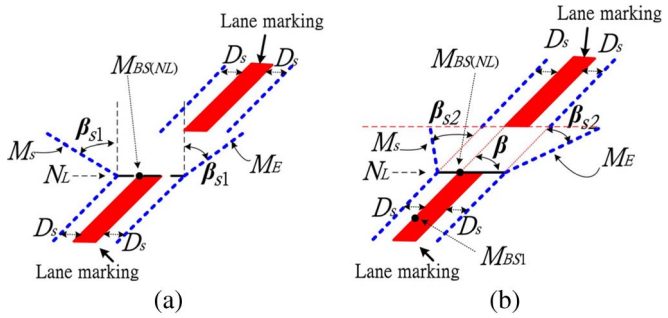

Fig. 9. (a) Bidirectional expansion scheme. (b) Tendency expansion scheme.

direction of the N-coordinate to determine the ROI. The computation method of the slope is shown in Fig. 9(b), where m_b denotes the slope of the lane marking. If a BFT is detected continuously in some rows, but cannot be detected in the following several consecutive rows, then let $M_{BS(NL)}$ be the BS on the latest BFT and let M_{BS1} be the BS on the BFT in the previous rows of $M_{BS(NL)}$. Then, the slope of the lane markings can be computed using these two points. With the slope, the ROI can be determined by (16) and (17). The ROI calculated in this way is smaller, where the lane marking is included; however, the computational cost of the slope may increase.

$$M_L = \left(M_{BS(NL)} - D_s\right) - (N_p - N_L) \times \tan(\beta_{s1}) \quad (14)$$

where

$M_{BS(NL)}$	M-coordinate of BS in the N_L row;
N_L	row where BFT is latest detected;
D_s	fixed shift range;
β_{s1}	fixed angle of expansion.

$$M_R = \left(M_{BT(NL)} + D_s\right) + (N_p - N_L) \times \tan(\beta_{s1}) \quad (15)$$

where

$M_{BT(NL)}$	M-coordinate of BT in the N_L row.

$$M_L = \left(M_{BS(NL)} - D_s\right) + (N_p - N_L)/m_L \quad (16)$$

where

$M_{BS(NL)}$	$= (m_{BS}, N_L)$;
m_{BS}	denotes the M-coordinate of BS;
$M_{BS1} = (m_1, n_1)$	represents another M_{BS};
β	$= \tan^{-1}\left(\frac{N_L - n_1}{m_{BS} - m_1}\right)$;
m_L	$= \tan(\beta + \beta_{s2})$;
β_{s2}	fixed angle of expansion.

$$M_R = \left(M_{BT(NL)} + D_s\right) + (N_p - N_L)/m_R \quad (17)$$

where

m_R	$= \tan(\beta - \beta_{s2})$.

3) Tracking Approach: Based on the lane marking features found in previous frames, the ROI can be found by (18) and (19). The ROI area found in this way is the smallest one, so it is the best choice for the sequential prediction mode of lane detection

$$M_L = M_{BS(t-1)} - D_s \quad (18)$$

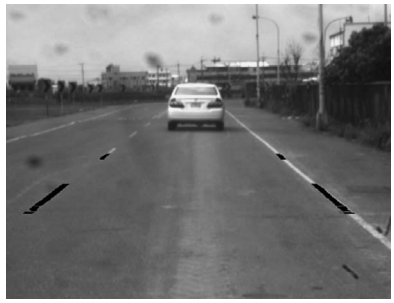

Fig. 10. Acquisition of BFT in a fixed area.

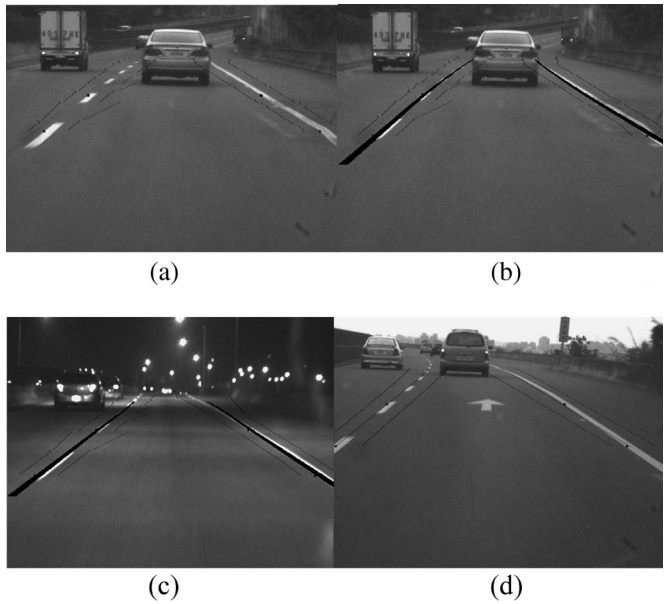

Fig. 11. Select of ROI and its range. (a)–(c) The application of the expansion approach. (d) The adoption of the tracking approach.

where

$M_{BS(t-1)}$	M-coordinate of BS in the N_p row in the previous frame;
t	current frame, and $t-1$ is the last frame.

$$M_R = M_{BT(t-1)} + D_s \quad (19)$$

where

$M_{BT(t-1)}$	M-coordinate of BT in the N_p row in the previous frame.

Fig. 10 shows the acquisition of BFT in a fixed area. The detection distance is set to be about 25 m. In the figure, black lines appear only when the distance between BFT on both sides approximates to w_L. Fig. 11 shows the selection of the ROI and its range. In (a), (b) and (c), the two-side expansion phase and tendency expansion phase are applied in turn, while the tracking approach is adopted in (d). In Fig. 11, the black lines on the two sides of the lane markings, respectively, represent M_L and M_R of those rows. On the lane markings of both sides, there are totally four big black points that denote P_{L1}, P_{L2}, P_{R1}, and P_{R2} for calibrating α.

D. Postprocessing by Fuzzy Reasoning

Some objects or noises whose features are similar to those of lane markings may exist in the image, so they may also be extracted simultaneously. In this paper, a postprocessing scheme based on fuzzy logic is adopted to determine whether the potential objects are actual lane markings in the extracted image. The following rules are applied to the identification of lane markings.

1) When the length of BFT $B_L(N)$ detected in the Nth row of the image approximates closer to the computed width of the lane markings $w_m(N)$, the BFT has a higher possibility of being part of the lane markings. A triangular fuzzy number is used as a membership grade μ_1 to represent the degrees of their similarity as in (20), shown at the bottom of the page, where $B_L(N)$ means the length of BFT first detected by FSM in the Nth row and $w_m(N)$ denotes the width of the lane marking projected on the Nth row by (6). The notation $\mu_1(N)$ represents the degrees of similarity between $w_m(N)$ and $B_L(N)$. The larger the membership grade is, the higher possibility it is for the detected BFT to be part of the actual lane markings. Otherwise, a smaller membership grade reveals that the detected BFT may just be noise.
2) Given a row on the image plane, a pair of BFTs is detected within ROI of both the left and right lane markings, and then, the two BFTs may possibly be parts of the lane markings. The possibility rises with the distance between the two BFTs D_B getting more close to the computed width of the projected lane marking w_L. The notation $\mu_2(N)$ represents the degrees of similarity between D_B and w_L in (21), shown at the bottom of the page, where $D_B(N)$ represents the distance between two BFTs on the Nth row and $w_L(N)$ means the projective lane width on the Nth row by (3). $\mu_2(N)$ denotes the similarity between $D_B(N)$ and $w_L(N)$.
3) Suppose that all lane markings are longitudinally consistent; thus, the BFT detected within the ROI on the left or right lane markings should be parts of them. Let the range of the projective lane markings be the rows of $[0, N_e]$ on the N-coordinate, then each BFT detected within the area can obtain a membership grade μ_1. Let a fuzzy set F_M denote the set of μ_1 on the same lane marking as in (22). All membership grades in F_M should be similar since they belong to the BFT on the same lane marking. Therefore, if μ_1 of one BFT matches the condition in (23), then the BFT is regarded as a part of the lane marking; otherwise, it is noise

$$F_M = \{(N, \mu_1(N)) \,|N \in [0, N_e]\} \tag{22}$$

where N_e represents the preset terminal row.

$$|\mu_1(N) - \mu_m| \leq \sigma_1^2 \tag{23}$$

where μ_m is the mean of $\mu_1(N)$ in fuzzy set F_M and σ_1^2 is the variance of $\mu_1(N)$ in fuzzy set F_M.
4) Let lane projections be within the range $[0, N_e]$ in the N-coordinate. If BFT is detected within the left and right areas of the ROI, then $\mu_2(N)$ can be obtain by (21). Let fuzzy set F_L denote the set of μ_2 on the same lane as in (24). Supposing that changes of lane width are slight, then each $\mu_2(N)$ computed based on the BFT should be similar. The existence of lane markings on both sides in the N row is determined by (25) and $\mu_2(N)$. Accordingly, whether lane markings exist on both sides can be determined. Moreover, search the BFTs on the same lane marking which meet rule 3, and next, compute the associated Z-coordinates of those BFTs' v-coordinates by (1). If the Z-coordinates between two neighboring BFTs exceed 10 m, it means that the area between them is occluded. Then, one side of the lane marking should be compensated by the other side

$$F_L = \{(N, \mu_2(N)) \,|N \in [0, N_e]\} \tag{24}$$

$$|\mu_2(N) - \mu_{2m}| \leq \sigma_2^2 \tag{25}$$

where μ_{2m} is the mean of $\mu_2(N)$ in the fuzzy set F_L and σ_2^2 is the variance of $\mu_2(N)$ in the fuzzy set F_L.

The application of the rules is described as follows: First, compute $\mu_1(N)$ and $\mu_2(N)$ by rules 1 and 2. Then, choose the BFT which satisfies most conditions of lane markings by rule 3. Next, rule 4 is applied to judge whether there is any occlusion on the left and right lane markings. Finally, determine the positions of knots based on rules 3 and 4 to reconstruct the lane as shown in the following section.

$$\mu_1(N) = \begin{cases} (B_L(N) - w_m(N))/w_m(N) + 1, & \text{if } 0 \leq B_L(N) \leq w_m(N) \\ -(B_L(N) - w_m(N))/w_m(N) + 1, & \text{if } w_m(N) \leq B_L(N) \leq 2 \times w_m(N) \\ 0, & \text{otherwise} \end{cases} \tag{20}$$

$$\mu_2(N) = \begin{cases} 2 \times (D_B(N) - w_L(N))/w_L(N) + 1, & \text{if } 0.5 \times w_L(N) \leq D_B(N) \leq w_L(N) \\ -2 \times (D_B(N) - w_L(N))/w_L(N) + 1, & \text{if } w_L(N) \leq D_B(N) \leq 1.5 \times w_L(N) \\ 0, & \text{otherwise} \end{cases} \tag{21}$$

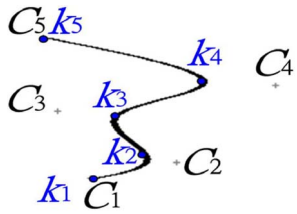

Fig. 12. B-spline model for lane marking detection.

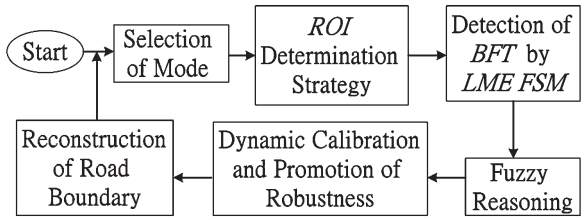

Fig. 13. Procedures of the lane marking detection.

E. Reconstruction Process of Occluded Lanes

Some lane markings are dashed lines, and some may be occluded by obstacles; thus, the detected lane markings cannot completely reveal the driving lane in the whole area. To overcome these issues, the B-spline technique is used to interpolate the positions of lane markings to obtain the complete lane boundaries. The cubic B-spline is a smooth curve with continuous second-order derivatives [40], [42]–[44], fitting curves of various lane markings by using several control points.

1) Decision of Control Points: Let C_i be the ith control point in the control point set C_s, as expressed in (26), and then, the cubic B-spline is $B(s)$, as shown in (27), which contains connected curve segments $g_i(s)$

$$C_s = \{C_i | i = 1, 2, \ldots, n\} \tag{26}$$

where the coordinates of C_i are (M_i, N_i). M_i and N_i, respectively, represent the M-coordinate and N-coordinate in the image. i ranges from 1 to n, which means that the number of control points is n

$$B(s) = \sum_i g_i(s), \qquad 0 \le s \le 1 \tag{27}$$

where

$$g_i(s) = (M_i(s), N_i(s)) = [s^3 + s^2 + s + 1] \begin{bmatrix} -\frac{1}{6} & \frac{1}{2} & -\frac{1}{2} & \frac{1}{6} \\ \frac{1}{2} & -1 & \frac{1}{2} & 0 \\ -\frac{1}{2} & 0 & \frac{1}{2} & 0 \\ \frac{1}{6} & \frac{2}{3} & \frac{1}{6} & 0 \end{bmatrix} \begin{bmatrix} C_{i-1} \\ C_i \\ C_{i+1} \\ C_{i+2} \end{bmatrix}$$

with $i = 2, 3, \ldots, n-2$. The range of i is from 2 to $n-2$, which shows that, when there are n control points, the number of curves is $n-3$. s is a normalized curve length.

Lane markings may appear in straight lines, curves, and even S-shape turns. Therefore, it is difficult to completely model lane markings with various forms with linear or quadratic equation models. In this paper, a B-spline of four connected curve segments $g_i(s)$ is applied to fitting the curved lane markings. A variety of lane markings with general characteristics can be modeled by this approach. To enable B-spline to go through the first and last control points, the two control points are repeated three times. Five control points are determined to be C_1, C_1, C_1, C_2, C_3, C_4, C_5, C_5, C_5 as shown in Fig. 12. The connected points of the curves are named knot points. The positions of the control points can be determined according to those of the knot points. Substituting $s = 0$ into (27), the results in (28) can be obtained. Then, based on (28), three knot points k_2, k_3, and k_4 on the lane marking are selected between C_1 and C_5 to obtain three control points C_2, C_3, and C_4 as shown in (29)

$$C_i = \frac{3}{2}k_i - \frac{1}{4} \times (C_{i-1} + C_{i+1}) \tag{28}$$

where $i = 2, 3, \ldots, n-2$,

$$\begin{bmatrix} C_2 \\ C_3 \\ C_4 \end{bmatrix} = \begin{bmatrix} -\frac{15}{56} & \frac{45}{28} & -\frac{3}{7} & \frac{3}{28} & -\frac{1}{56} \\ \frac{1}{14} & -\frac{3}{7} & \frac{12}{7} & -\frac{3}{7} & \frac{1}{14} \\ -\frac{1}{56} & \frac{3}{28} & -\frac{3}{7} & \frac{45}{28} & -\frac{15}{56} \end{bmatrix} \begin{bmatrix} C_1 \\ k_2 \\ k_3 \\ k_4 \\ C_5 \end{bmatrix}. \tag{29}$$

2) Decision of Knot Points: In this paper, a lane marking is formed by connecting five knot points using B-spline. The position of the second knot point k_2 is selected by the mapping position in the image of the lane marking near the Z-coordinate = 10 m; in the third knot k_3, the associated Z-coordinate is about 25 m. The lines passing through k_3 and k_2 intersect at the bottom row of the image coordinate, and the associated intersection is denoted by k_1. Knot 5 is at the end of the lane marking, and knot 4 is chosen from a suitable place between knots 3 and 5 which is the most probable position of a BFT on a lane marking by fuzzy rule. Knots 1 and 5 are determined by this way as well, and they are the control points C_1 and C_5.

F. Overall Process of Lane Detection

In single mode, the fixed area ROI approach is first applied to the LME FSM process to extract lane markings. After lane markings are found, the lane width and the tilt angle of the camera are updated by the dynamic calibration process, and then, the expansion ROI approach is applied again to extracting lane markings. This process can provide more accurate detection results. Because the calibration of the camera tilt angle and lane widths requires information of two lane markings, therefore, in the single mode, the information of the two lane markings in the fixed ROI is needed. If only the information of the left or right lane marking is available, it is possible that one side of the lane marking is occluded. The information of this occluded lane marking can be compensated by the information of the previously detected lane width and the other side of the lane marking. The procedures are shown in Fig. 13.

Step 1) Selection of Modes: Apply the sequential mode when the previous information is logical and adequate; otherwise, use the single mode.
Step 2) ROI determination strategy.
Step 3) Detection of BFT by LME FSM.

TABLE II
COMPUTATION TIMINGS UNDER DIFFERENT CONDITIONS BY THE PROPOSED SYSTEM

Conditions	The number of frames	Average computation time	Detection rate
Straight road	3500	4.5 ms	99.1%
Curve road	2200	7.3 ms	98.7%
Daytime occluded	1250	12.2 ms	96.4%
Shadow	1100	9.5 ms	96.5%
Strong sunlight	500	9.3 ms	97.2%
Night	2100	7.2ms	98.3%
Night occluded	1200	12.9 ms	95.1%

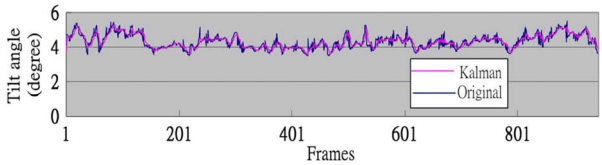

Fig. 14. Result of the dynamic calibration of camera's tilt angle.

Step 4) Fuzzy reasoning: Determine the points used to calibrate the tilt angle of the camera and the knots adopted to reconstruct road boundaries.

Step 5) Dynamic calibration and promotion of robustness: Apply dynamic calibration to obtain the actual tilt angle of camera and lane width. Then, apply the Kalman filters to stabilize the calibration results.

Step 6) Reconstruction of road boundaries: Reconstruct road boundaries using B-spline, and then, go back to Step 1).

IV. EXPERIMENTAL RESULTS

In this section, comparative experiments on lane detection are conducted. This paper utilizes a Hitachi KP-F3 camera mounted in an experimental intelligent car with a physical pixel size of 7.4 μm(H) $\times$ 7.4 μm(V), and the image resolution is 644 $\times$ 493. The height of the camera is set at 1.32 m, the focal length $f = 15$ mm, and tilt angle α is about 4°. Our experimental system is a PC with CPU Pentium IV 2.8 GHz. Suppose that the width of the lane marking is 0.1 m and the initial lane width is 3.3 m. The farthest distance of detection is 60 m, and the associated computed projective width of the lane marking is about 5 pixels. The experimental conditions and results are shown in Table II. The average computation time that the proposed method required is less than 13 ms per frame. Under general conditions, the average detection rate can reach above 98% and exceed 95% when there are occlusions.

A. Lane Detection Results

1) Dynamic Calibration of Camera Tilt Angle: Fig. 14 shows the result of the dynamic calibration of camera's tilt angle. In the figure, "Original" means the calculated tilt angle in each frame. "Kalman" denotes the processed tilt angle by a Kalman filter. The Kalman filter can provide the robust estimation of the current tilt angles through recursive functions [45], [46]. This process provides the more stable and robust calibration results of the tilt angle for the lane detection system. Fig. 14 shows that the change of "Kalman" gets smaller.

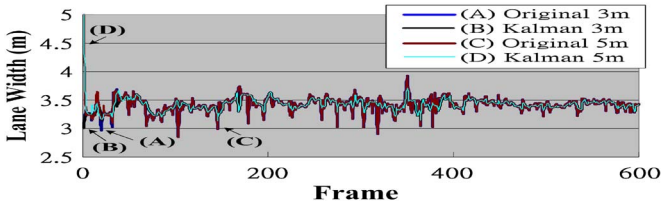

Fig. 15. Estimated lane width in every frame.

TABLE III
RESULTS OF LANE WIDTH ESTIMATION IN THE FOUR SITUATIONS

Curve	(A)	(B)	(C)	(D)
Mean (m)	3.422	3.421	3.423	3.424
Standard deviation (m)	0.1221	0.0874	0.1217	0.0885
Average error (m)	0.022	0.021	0.023	0.024

2) Lane Width Refinement: In lane detection, the initial settings are based on general width of lanes, i.e., 3–5 m, and the actual lane widths will later be adaptively refined based on the detected positions of the left and right lane markings in the image. Moreover, to promote the robustness of lane width refinement, a Kalman filter is also adopted to stabilize and refine the process of lane width estimation.

Fig. 15 shows the estimated lane widths with different preset widths and with/without Kalman filters in the sequential frames, where curves "(A) original 3 m" and "(C) original 5 m," respectively, represent the estimated lane widths with initial lane widths in 3 and 5 m. The initial lane widths of curves (A) and (C) were, respectively, set to be 3 and 5 m. The curves "(B) Kalman 3 m" and "(D) Kalman 5 m," respectively, denote the estimated lane widths of curves (A) and (C) refined by the Kalman filter. By observing those results, the estimated lane widths with different preset lane widths will finally be refined to be closer to the actual ones. The application of the Kalman filter ensures stable and robust estimate results of the lane widths in the world coordinates. Table III displays the mean, standard deviation, and average errors of the estimated lane widths in curves (A), (B), (C), and (D), and the actual lane width is about 3.4 m. As can be seen, the estimated results in sequential frames are all quite close to the actual lane width, and all of the average errors are under 0.024 m. Furthermore, when the initially set lane width changes within the range of 3–5 m, the obtained estimation results are still similar and close to the actual lane widths. The results show that our approach of lane width refining is robust and accurate.

3) Results of Adaptation to Illumination Conditions: D_{g1}, D_{g2}, and D_{g12} are determined by a statistical search algorithm based on the following two principles: 1) All gray levels of lane markings are higher than those of the ground, and 2) the variations of the gray levels of the ground and lane markings are within a reasonably fixed range. To demonstrate that our approaches are robust and adaptive to changes of illumination, variations of the gray levels of lane markings and grounds under four different illuminations are analyzed. The results are shown

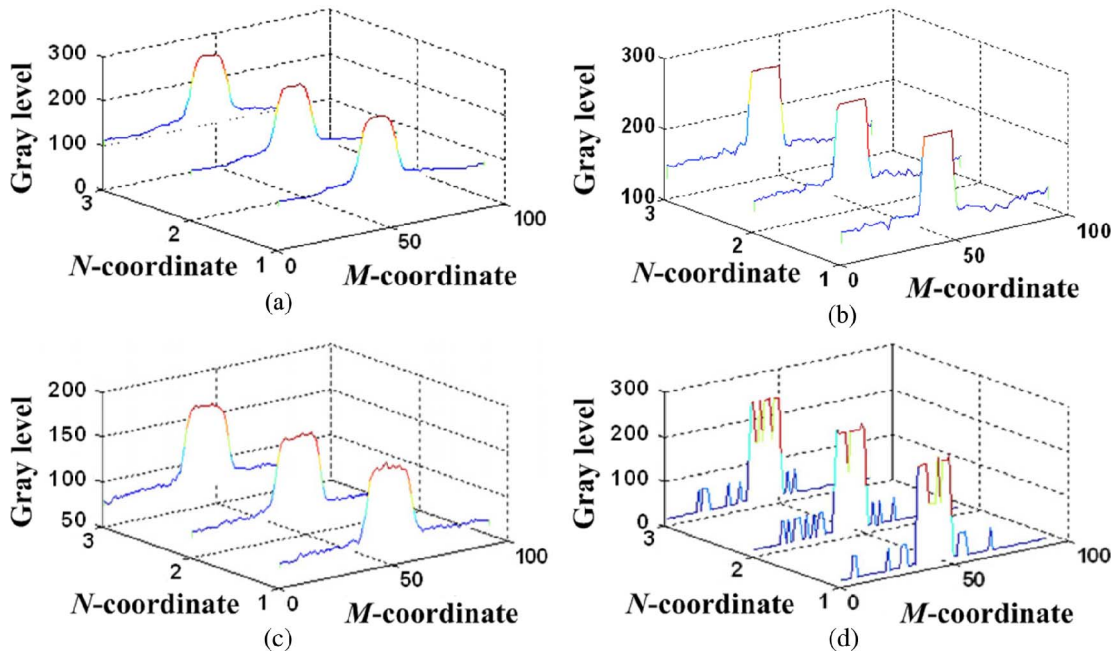

Fig. 16. Gray level of lane markings under different illumination. (a) General light. (b) Strong sunshine. (c) Dusk. (d) Night.

TABLE IV
OBTAINED PARAMETERS UNDER DIFFERENT ILLUMINATION CONDITIONS

Illumination conditions	D_{g1}	D_{g2}	D_{g12}
(a)General light	35	60	55
(b)Strong sunshine	30	10	85
(c)Dusk	25	20	50
(d)Night	70	110	75

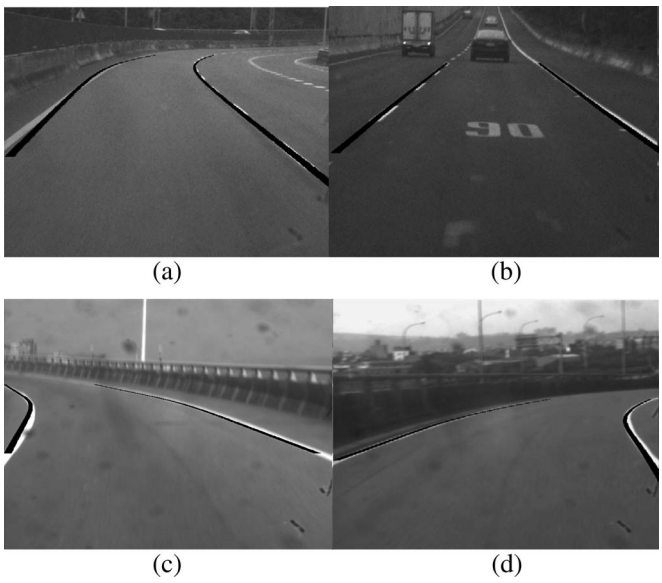

Fig. 17. (a) Curves. (b) A slope. (c) and (d) A cloverleaf interchange.

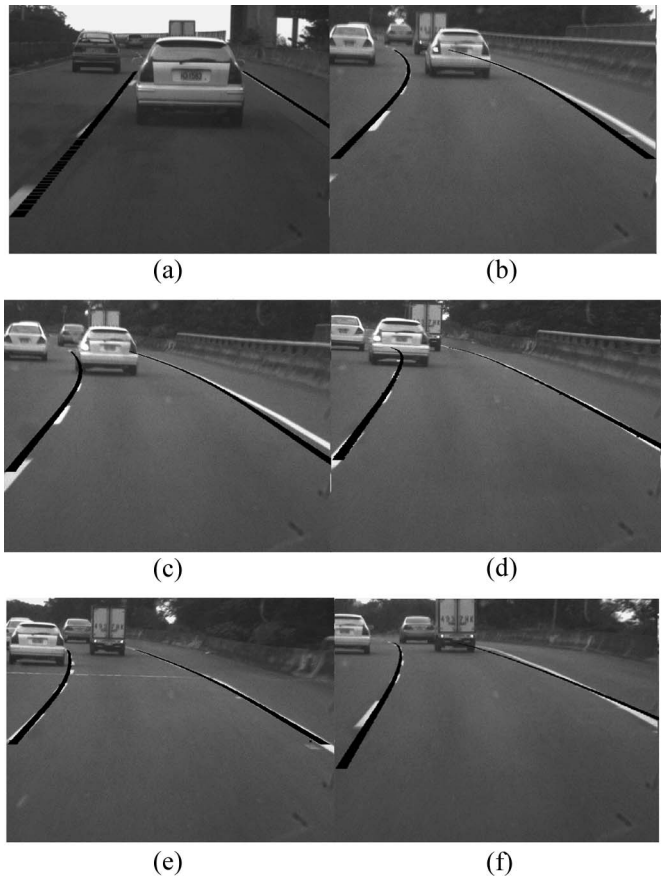

Fig. 18. (a)–(f) Situations of occlusion with different obstacles.

in Fig. 16, where lanes and lane markings display the different gray level and contrast under different illumination. As can be seen from this fact, the principles 1) and 2) are appropriately followed under different illumination conditions, and the proposed statistical search algorithm can correctly and adaptively determine D_{g1}, D_{g2}, and D_{g12} under various illumination conditions. Table IV displays D_{g1}, D_{g2}, and D_{g12} obtained from the four sample road scenes under different illumination conditions in Fig. 16, where D_{g1}, D_{g2}, and D_{g12} are adaptively adjusted with various illuminations. As shown in Figs. 17–21, the adaptively determined thresholds can provide satisfactory lane detection results under different illumination conditions.

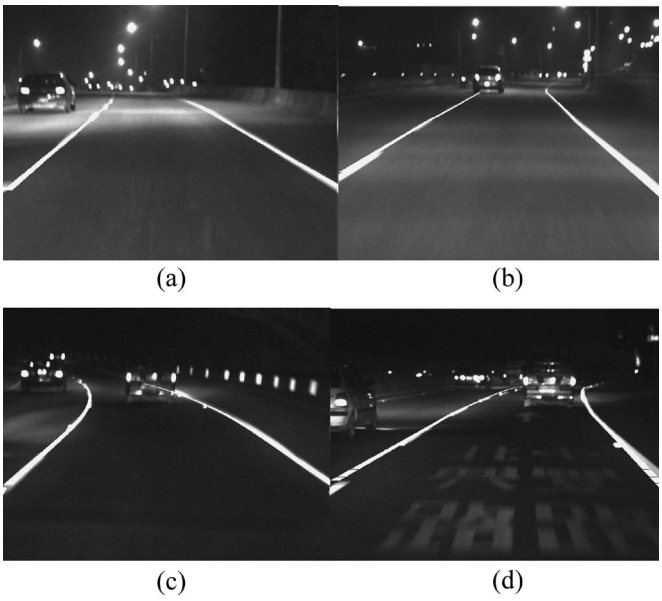

Fig. 19. Results of the nighttime road scene. (a) and (b) With road lamps. (c) and (d) Without road lamps.

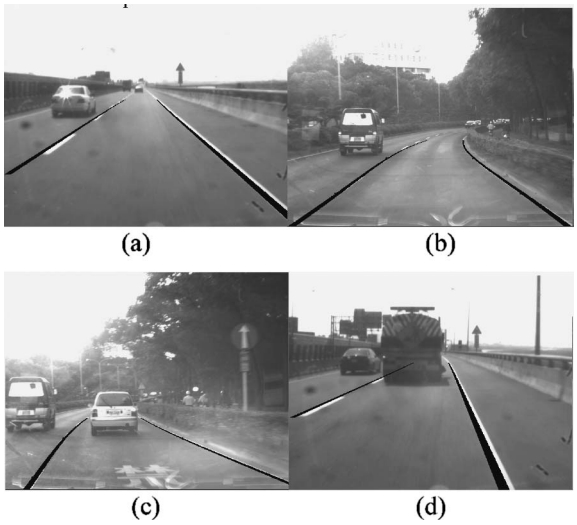

Fig. 20. Detection results under strong sunlight. (a) and (b) No occlusion of vehicles. (c) and (d) With the occlusion of a vehicle.

Fig. 17 shows the conditions of curves and a slope. In these figures, the roads with sharp curves and slopes can still be described by B-spline with four segments. Fig. 18 shows the situations with occlusion of obstacles, where the near front vehicle occluded lane markings of both sides (a), the vehicle occluded the right lane marking (b), the vehicle moved back to the road center (c), the vehicle occluded the left lane marking (d), the vehicles approached lane markings (e), and another vehicle occluded the right lane marking (f). The figures prove that the problem of occlusion can be solved by the proposed approaches. The information of the side which is not occluded can be used to substitute the occluded one. When both sides of the lane markings are occluded, then only the parts that are not occluded can be shown. Fig. 19 shows the detection results at night in situations including roads with or without road lamps and textures on the road surface, and roads with curves

Fig. 21. Detection result of a motorcycle inside and outside the lane. (a) Inside. (b) Outside.

Fig. 22. Results of the road scene that the lane markings are occluded with shadows, signs of braking. (a) Results of Jung and Kelber's approach [28]. (b) Results of the proposed approach.

and occlusion. Figs. 17–19 show that FSM can extract BFT in various situations regardless of the influences of patterns on the road surface and illumination, and B-spline with four sections is able to display a variety of road conditions. Fig. 20 shows the detection result under strong sunlight. The proposed approach can correctly detect the lane markings without being influenced by the strong sunlight. Fig. 21(a) and (b) shows a clear discrimination of a motorcycle inside and outside the lane, respectively. Obstacles inside the lane will affect driving safety. However, most contemporary lane detection approaches may not be able to discriminate whether an obstacle is inside or outside the lane when obstacles appear near the lane, so they cannot correctly detect lane markings. In contrast, the proposed approach can resolve the problem of obstacle occlusion to reconstruct correct lane markings.

B. Comparative Performance Evaluation

In this section, comparative experiments on Jung and Kelber's method [28] and the proposed approach are conducted to evaluate their performances on lane detection under different conditions. The following is a comparison of acquiring BFT by FSM and other approaches.

Figs. 22–26 show the comparative results of Jung and Kelber's [28] and our proposed approaches under different situations, where (a) is Jung and Kelber's approach and (b) is our proposed approach. Fig. 22 shows the condition that the lane markings are occluded with shadows, signs of braking, and other vehicles. Jung and Kelber adopted Sobel edge features of lane boundaries, which left large gradient points in the thresholded edge image, as shown in Fig. 22(a), where the surrounding vehicle may cause false detection in the edge feature

(a) (b)

Fig. 23. Results of road scenes with a curve lane and occlusion. (a) Results of Jung and Kelber's approach [28]. (b) Results of the proposed approach.

(a) (b)

Fig. 24. Results of the road scene under strong sunlight. (a) Results of Jung and Kelber's approach [28]. (b) Results of the proposed approach.

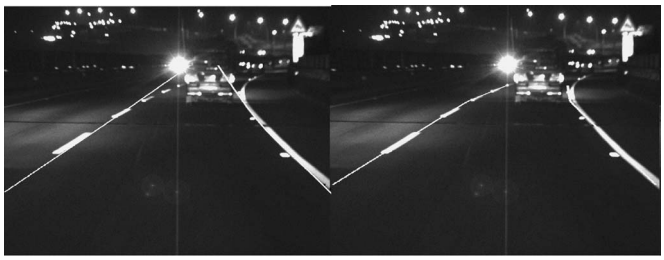

(a) (b)

Fig. 25. Results of the nighttime road scene. (a) Results of Jung and Kelber's approach [28]. (b) Results of the proposed approach.

extraction process and result in detective errors. As shown in Fig. 22(b), the proposed approach successfully extracts features of lane markings with the BFT detector. The end part of the reconstructed lane boundary is the position of the last BFT, and the missing part at the end of the left-side lane marking is reconstructed with the information of the lane width and of the right-side lane marking.

Fig. 23 shows the results of the road scene consisted of curve lane and occlusion. Fig. 23(a) shows that the lane markings obtained by Jung and Kelber's method have errors occurring on curves of roads when edge features of vehicles are misdetected as the lane markings. Fig. 23(b) shows that our BFT approach can compensate the influences of appearing vehicles. Fig. 24 shows the detection results under strong sunlight. In Fig. 24(a), the edge features of vehicles associated with significant gradient features under strong sunlight cause possibly wrong determination of lane features. As shown in Fig. 24(b), with the BFT method, the proposed approach will not capture positions without lane markings to avoid wrong judgments in the far end of the lane. Therefore, lane boundaries can be reconstructed successfully.

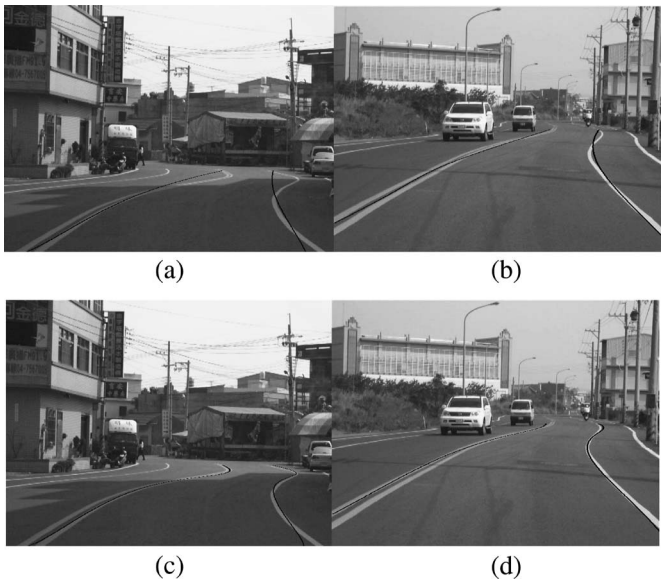

(a) (b) (c) (d)

Fig. 26. Results of the road scene with an S-shaped lane. (a) and (b) Results of Jung and Kelber's approach [28]. (c) and (d) Results of the proposed approach.

Fig. 25 shows the detection results at night. In Fig. 25(a), larger gradient arouses detection errors because of the opposite vehicle light and the light reflection of the preceding vehicle. The proposed approach can detect lane markings efficiently and correctly, as shown in Fig. 25(b), because it takes projective sizes and sequences of lane markings into consideration in capturing BFT.

Fig. 26 shows the detection results of the road scene with an S-shape lane. In Fig. 26(a), the S-shaped lane cannot be completely reconstructed when Jung and Kelber applied a linear-parabolic model to reconstruct lane boundaries. Fig. 26(b) shows that the proposed approach can successfully reconstruct the S-shaped lane boundary.

As can be seen from the aforementioned comparative results, the proposed approach can obtain satisfactory detection results under different situations, such as different illumination conditions, curve roads, and occlusions. This is because lane markings are extracted by the proposed BFT detector and the extraction errors can be effectively reduced by the proposed dynamic calibration method, ROI determination strategy, and fuzzy rule-based scheme, and road boundaries are effectively reconstructed by the B-spline technique. Moreover, when both sides of lane markings do not exist, or are occluded at the farther parts of the road, the range of the reconstructed lane is determined by the actual visible position of the lane, so the information obtained from previous frames will not be misused to reconstruct false lanes and driving safety can be improved.

C. Comparative Analysis

In this section, a comparative analysis on the methods of Jung and Kelber [28], Jeong and Nedevschi [25], Cheng *et al.* [39], and the proposed method is provided as shown in Table V. Cheng *et al.* adopted a color camera, while others used monochrome cameras. The color camera is able to obtain information on colors in the images, but it costs more and takes more time to process more information.

TABLE V
COMPARISON OF DIFFERENT ALGORITHMS

method	Camera type	Extraction method	Dynamic calibration	Occlusion handling	Computation cost	Illumination condition adapting
Jung and Kelber [28]	monochrome	Sobel mask and Hough Transform	N/A	poor	High	Fair
Jeong and Nedevschi [25]	monochrome	Gabor filter	N/A	poor	High	Fair
Cheng *et al*. [39]	color	Multivariable Gaussian distributions	Tilt	Fair	Medium	Fair
Our proposed method	monochrome	*LME FSM* + *ROI* strategy	Tilt, width of lane	Good	Low	Good

As to the extraction methods, Jung and Kelber [28] used a Sobel mask to conduct edge extraction, in which processing one pixel required ten additions, four multiplications, and a Hough transform to carry out line detection, so this method suffers high computation cost. Jeong and Nedevschi [25] applied a Gabor filter, which required complicated computational cost for exponential and trigonometric functions. Cheng *et al.* [39] adopted three multivariable Gaussian distributions to show three classes of lane-mark colors and computed the probability distribution of pixels belonging to the lane-mark, which also involved more complicated computations to analyze three color classes. The proposed LME FSM needs only simple linear equation in every row to determine widths of lanes and lane markings, and it only requires one subtraction to calculate the difference in gray level of each pixel. Therefore, the computation cost is the smallest and is applicable to an embedded system. The proposed ROI could effectively choose a suitable strategy to narrow down the detection area and greatly reduce the time for detection. Furthermore, only the proposed approaches obtained both the camera tilt angle and the lane width with the information of images and solved the problem of moving camera vibrations and occlusion on the lane marking without the information of colors. Moreover, the proposed approach adopts the statistical search algorithm to determine the gray-level range of ground and lane markings, so it enables BFT detector to effectively extract lane markings in various conditions of illumination.

V. CONCLUSION

To apply lane detection for the guidance of autonomous vehicles and driving assistance system, a variety of road conditions should be considered, such as changes of illumination, a great diversity of road curvature, and difference in the configurations of lane markings like continuous, dashed, or occluded road markings. A lane detection system should have high efficiency, robustness, and reliability to make driving at high speed safe.

This paper has proposed a rapid computation of lane width to predict the projective positions and widths of lane markings, and an approach LME FSM is designed to extract lane markings efficiently. A statistical search algorithm is also proposed to correctly and adaptively determine thresholds under various kinds of illumination conditions. Moreover, a dynamic calibration algorithm is applied to update the information of a camera's parameters and lane width. In addition, a method of fuzzy reasoning is adopted to determine whether the lane marking is continuous, dashed, or occluded. Finally, the strategy of the ROI is proposed to narrow the search region and make the detection more robust. The experimental results show that even when obstacles occlude parts of the lane markings or lane markings have complicated curvature, road boundaries still can be reconstructed correctly by B-spline with four segments. In conclusion, even with the information of lanes, there are still many threats from surrounding vehicles and obstacles when driving. Thus, the function of obstacle detection should be combined with lane detection systems to make the guidance of autonomous vehicles and driving assistance systems better in the future.

APPENDIX A
RELATION OF PROJECTED WIDTH AND V-COORDINATE

If the lane width is W_{WL} and the projective lane width on the v-coordinate is $w_L(v)$, then (A-1) can be obtained from (1) and (2). Equation (A-2) means the first derivative for v to $w_L(v)$. Let $\xi = (\pi/2 - \alpha)$, and $\tau = \tan^{-1}(v/\lambda)$. Then, (A-4) and (A-5) can be derived from (A-2) and (A-3). Since the camera was placed in a vehicle to detect the lane, when α is large, the farther part of the lane would not appear in the image. Therefore, α is usually between 0° and 6°. In this paper, let the tilt angle $\alpha < 10°$, and then, the value of ξ will be larger than 80°, and they are substituted in (A-6) and (A-7). Next, they are applied to (A-5) to obtain (A-8) and (A-9). Equation (A-9) shows that the first derivative of $w_L(v)$ is a constant. The relation between $w_L(v)$ and v can be expressed by a linear equation such as (3)

$$W_L(v) = \frac{W_{wL} \times \lambda}{h \cdot \tan\left(\left(\frac{\pi}{2} - \alpha\right) - \tan^{-1}\left(\frac{v}{\lambda}\right)\right)} \tag{A-1}$$

$$\frac{dW_L(v)}{dv} = \frac{W_{wL} \times \lambda}{h} \times \left(d\cot\left(\left(\frac{\pi}{2} - \alpha\right) - \tan^{-1}\left(\frac{v}{\lambda}\right)\right) \Big/ dv\right) \tag{A-2}$$

$$\cot(\xi - \tau) = \frac{1 + \tan(\xi) \times \tan(\tau)}{\tan(\xi) - \tan(\tau)} \tag{A-3}$$

$$\frac{dW_L(v)}{dv} = \frac{W_{WL} \times \lambda}{h} \times \left(\kappa \times \frac{d\omega}{dv} - \omega \times \frac{d\kappa}{dv}\right) \Big/ \kappa^2 \tag{A-4}$$

where $\omega = 1 + \tan(\xi) \times \tan(\tau)$; $\kappa = \tan(\xi) \times \tan(\tau)$,

$$\frac{dW_L(v)}{dv} = \frac{W_{WL} \times \lambda}{h} \times \frac{\left(\tan(\xi) - \frac{v}{\lambda}\right) \times \frac{\tan(\xi)}{\lambda} - \left(1 + \tan(\xi) \times \frac{v}{\lambda}\right) \times \left(-\frac{1}{\lambda}\right)}{\left(\tan(\xi) - \frac{v}{\lambda}\right)^2} \tag{A-5}$$

$$\tan(\xi) \gg \frac{v}{\lambda} \tag{A-6}$$

$$\tan(\xi) \times \frac{\tan(\xi)}{\lambda} \gg \left(\frac{v}{\lambda^2} \times \tan(\xi) + \frac{1}{\lambda}\right) \tag{A-7}$$

$$\frac{dW_L(v)}{dv} \approx \frac{W_{WL} \times \lambda}{h} \times \frac{(\tan(\xi)) \times \frac{\tan(\xi)}{\lambda}}{(\tan(\xi))^2} \tag{A-8}$$

$$\frac{dW_L(v)}{dv} \approx \frac{W_{WL}}{h}. \tag{A-9}$$

APPENDIX B
ADAPTATION TO ILLUMINATION CONDITIONS

The proposed statistical search algorithm determines G_{gH}, G_{gL}, G_{mH}, and G_{mL} in the ROI for detecting lane markings. The procedures for determining the thresholds in each row are given as follows.

Step 1) Setting search windows: Set a window in each Nth row to search for G_{gH}, G_{gL}, G_{mH}, and G_{mL}. The width of the search window on the Nth row $W_w(N)$ is shown as (B-1). Here, the left border of the search window is also the left border of the search region of the lane marking on the Nth row

$$W_w(N) = \begin{cases} 5 \times w_m(N), & \text{if } (S_R \geq 5 \times w_m(N)) \\ S_R, & \text{otherwise} \end{cases} \tag{B-1}$$

where $w_m(N)$ is the estimated width of the lane marking on the Nth row and S_R denotes the search region.

Step 2) Finding zone of lane marking and ground in the window: Since the gray levels of lane markings are obviously higher than those of the ground, the distribution of gray levels in a search window can be divided into three main zones if a row of lane markings appears close to the center of the search window. The three main zones in sequence are a lowland, a plateau, and again a lowland of gray-level groups. These three zones can be determined according to the representative bright and dark levels of the lane markings and the ground, which are, respectively, the average gray levels of lane markings and the ground. Let G denote the gray levels in M-coordinate in the search window, as shown in (B-2). Compute the pixel number of the lane marking and the ground in the window, respectively, A_m and A_g, by (B-3). Let a set L be the ordered gray levels of the pixels in G, which are arranged from large to small as in (B-4), where L_1 and L_{Aw}, respectively, represent the highest and lowest gray levels in G.

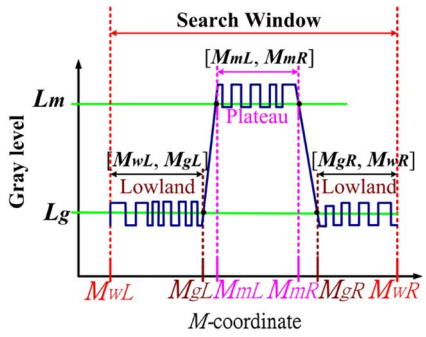

Fig. 27. Gray-level distribution with a row of lane marking in the search window.

L_m is the average gray level of lane markings, i.e., the average of the brightest A_m pixels with the highest gray level among the set L. L_g is the average gray levels of the ground, also the average of the darkest A_g pixels with the lowest gray level among L as shown in (B-5). After finding the representative bright and dark levels of the lane markings and the ground, three zones of interest can be found based on the following definitions. In the search window, the left and right borders of the lane marking, M_{mL} and M_{mR}, are respectively defined as the leftest and rightest pixel whose gray levels are larger than L_m. The left border of ground M_{gL} is defined as the pixel whose gray level is lower than L_g and being closest to M_{mL}. The right border of the ground M_{gR} is defined as the pixel with gray level lower than L_g and closest to M_{mR}. Fig. 27 shows the gray level of each pixel in G when a row of the lane marking exists in the search window. As can be seen, the plateau zone $[M_{mL}, M_{mR}]$ of the lane marking in G can be found by L_m, and the lowland zone, union of $[M_{wL}, M_{gL}]$ and $[M_{gR}, M_{wR}]$, of the ground can be found by L_g

$$G \triangleq \{G_M | M \in [M_{wL}, M_{wR}]\} \tag{B-2}$$

where G_M denotes the gray level in M-coordinate and M_{wL} and M_{wR}, respectively, represent the left and right boundaries of the search window

$$A_m = r_{mw} \times A_w \quad r_{mw} = \frac{w_m(N)}{W_w(N)} \quad A_g = A_w - A_m \tag{B-3}$$

where A_w is the number of pixels in the search window and r_{mw} denotes the ratio of $w_m(N)$ to $W_w(N)$

$$L \triangleq \{L_j | j \in [1, A_w]\} \tag{B-4}$$

$$L_m = \frac{1}{A_m} \sum_{j=1}^{A_m} L_j \quad L_g = \frac{1}{A_g} \sum_{j=A_m+1}^{A_w} L_j. \tag{B-5}$$

Step 3) Determining G_{mH}, G_{mL}, G_{gH}, and G_{gL}: Determine the highest and lowest gray levels in the plateau zone, G_{mH} and G_{mL}, using (B-6), and the

highest and lowest in the lowland zone, G_{gH} and G_{gL}, by (B-7)

$$G_{mH} \triangleq \max\{G_M | M \in [M_{mL}, M_{mR}]\}$$
$$G_{mL} \triangleq \min\{G_M | M \in [M_{mL}, M_{mR}]\} \quad \text{(B-6)}$$
$$G_{gH} \triangleq \max\{G_M | M \in \{[M_{wL}, M_{gL}] \cup [M_{gR}, M_{wR}]\}\}$$
$$G_{gL} \triangleq \min\{G_M | M \in \{[M_{wL}, M_{gL}] \cup [M_{gR}, M_{wR}]\}\}. \quad \text{(B-7)}$$

Step 4) Verifying G_{mH}, G_{mL}, G_{gH}, and G_{gL}: Check whether the determined G_{gH}, G_{gL}, G_{mH}, and G_{mL} are correct by verifying that G_{gH} is smaller than G_{mL}. If so, substitute G_{gH}, G_{gL}, G_{mH}, G_{mL} in (11) to obtain the corresponding D_{g1}, D_{g2}, D_{g12} on this row and go to step 6. Otherwise, go to step 5.

Step 5) Checking whether S_R is completely searched: If so, let D_{g1}, D_{g2}, D_{g12} in this row be the same as those in the previous row and go to step 6. Otherwise, shift the window rightward for the distance of $w_m(N)$ and return to Step 2).

Step 6) Terminate the determination process of the Nth row, and export the results of G_{mH}, G_{mL}, G_{gH}, and G_{gL}.

REFERENCES

[1] H. Takahashi, D. Ukishima, K. Kawamoto, and K. Hirota, "A study on predicting hazard factors for safe driving," *IEEE Trans. Ind. Electron.*, vol. 54, no. 2, pp. 781–789, Apr. 2007.

[2] M. Wada, K. S. Yoon, and H. Hashimoto, "Development of advanced parking assistance system," *IEEE Trans. Ind. Electron.*, vol. 50, no. 1, pp. 4–17, Feb. 2003.

[3] G. Ogawa, K. Kise, T. Torii, and T. Nagao, "Onboard evolutionary risk recognition system for automobiles—Toward the risk map system," *IEEE Trans. Ind. Electron.*, vol. 54, no. 2, pp. 878–886, Apr. 2007.

[4] T. Bucher, C. Curio, J. Edelbrunner, C. Igel, D. Kastrup, I. Leefken, G. Lorenz, A. Steinhage, and W. V. Seelen, "Image processing and behavior planning for intelligent vehicles," *IEEE Trans. Ind. Electron.*, vol. 50, no. 1, pp. 62–75, Feb. 2003.

[5] A. Kuma, "Computer-vision-based fabric defect detection: A survey," *IEEE Trans. Ind. Electron.*, vol. 55, no. 1, pp. 348–363, Jan. 2008.

[6] R. Chapuis, R. Aufrere, and F. Chausse, "Accurate road following and reconstruction by computer vision," *IEEE Trans. Intell. Transp. Syst.*, vol. 3, no. 4, pp. 261–270, Dec. 2002.

[7] R. Chapuis, R. Aufrere, and F. Chausse, "Robust lane detection and tracking for driving assistance systems," in *Proc. IEEE Syst., Man, Cybern. Symp.*, Oct. 2007, pp. 3848–3853.

[8] J. C. McCall and M. M. Trivedi, "Video-based lane estimation and tracking for driver assistance: Survey, system, and evaluation," *IEEE Trans. Intell. Transp. Syst.*, vol. 7, no. 1, pp. 20–37, Mar. 2006.

[9] B. F. Wu and C. T. Lin, "Real-time fuzzy vehicle detection based on contour size similarity," *Int. J. Fuzzy Syst.*, vol. 7, no. 2, pp. 54–62, Jun. 2005.

[10] B. F. Wu and C. T. Lin, "A fuzzy vehicle detection based on contour size similarity," in *Proc. IEEE Intell. Veh. Symp.*, Jun. 2005, pp. 496–501.

[11] S. Kim, J. H. Park, S. I. Cho, S. Park, K. Lee, and K. Choi, "Robust lane detection for video-based navigation systems," in *Proc. 19th IEEE Int. Conf. Tools Artif. Intell.*, Oct. 2007, pp. 535–538.

[12] E. D. Dickmanns and B. D. Mysliwetz, "Recursive 3-D road and relative ego-state recognition," *IEEE Trans. Pattern Anal. Mach. Intell.*, vol. 14, no. 2, pp. 199–213, Feb. 1992.

[13] A. Broggi, M. Bertozzi, C. Lo Guarino, and A. Bianco, "Visual perception of obstacles and vehicles for platooning," *IEEE Trans. Intell. Transp. Syst.*, vol. 1, no. 3, pp. 164–176, Sep. 2000.

[14] M. Bertozzi and A. Broggi, "GOLD: A parallel real-time stereo vision system for generic obstacle and lane detection," *IEEE Trans. Image Process.*, vol. 7, no. 1, pp. 62–81, Jan. 1998.

[15] C. Kreucher and S. Lakshmanan, "LANA: A lane extraction algorithm that uses frequency domain features," *IEEE Trans. Robot. Autom.*, vol. 15, no. 2, pp. 343–350, Apr. 1999.

[16] V. Kastrinaki, M. Zervakis, and K. Kalaizakis, "A survey of video processing techniques for traffic applications," *Image Vis. Comput.*, vol. 21, no. 4, pp. 359–381, Apr. 2003.

[17] T. N. Schoepflin and D. J. Dailey, "Dynamic camera calibration of roadside traffic management cameras for vehicle speed estimation," *IEEE Trans. Intell. Transp. Syst.*, vol. 4, no. 2, pp. 90–98, Jun. 2003.

[18] L. L. Wang and W. H. Tsai, "Camera calibration by vanishing lines for 3-D computer vision," *IEEE Trans. Pattern Anal. Mach. Intell.*, vol. 13, no. 4, pp. 370–376, Apr. 1991.

[19] B. F. Wu and C. T. Lin, "Robust image measurement and analysis based on perspective transformations," in *Proc. IEEE Syst., Man, Cybern. Symp.*, Oct. 2006, pp. 2390–2395.

[20] J. Wang, F. Shi, J. Zhang, and Y. Liu, "A new calibration model of camera lens distortion," *Pattern Recognit.*, vol. 41, no. 2, pp. 607–615, Feb. 2008.

[21] S. Nedevschi, C. Vancea, T. Marita, and T. Graf, "Online extrinsic parameters calibration for stereovision systems used in far-range detection vehicle applications," *IEEE Trans. Intell. Transp. Syst.*, vol. 8, no. 4, pp. 651–660, Dec. 2007.

[22] Y. Motai and A. Kosaka, "Hand-eye calibration applied to viewpoint selection for robotic vision," *IEEE Trans. Ind. Electron.*, vol. 55, no. 10, pp. 3731–3741, Oct. 2008.

[23] Y. M. Liang, H. R. Tyan, S. L. Chang, H. Y. M. Liao, and S. W. Chen, "Video stabilization for a camcorder mounted on a moving vehicle," *IEEE Trans. Veh. Technol.*, vol. 53, no. 6, pp. 1636–1648, Nov. 2004.

[24] P. Jeong and S. Nedevschi, "Local difference probability (LDP)-based environment adaptive algorithm for unmanned ground vehicle," *IEEE Trans. Intell. Transp. Syst.*, vol. 7, no. 3, pp. 282–292, Sep. 2006.

[25] P. Jeong and S. Nedevschi, "Efficient and robust classification method using combined feature vector for lane detection," *IEEE Trans. Circuits Syst. Video Technol.*, vol. 15, no. 4, pp. 528–537, Apr. 2005.

[26] Y. He, H. Wang, and B. Zhang, "Color-based road detection in urban traffic scenes," *IEEE Trans. Intell. Transp. Syst.*, vol. 5, no. 4, pp. 309–318, Dec. 2004.

[27] B. Fardi and G. Wanielik, "Hough transformation based approach for road border detection in infrared images," in *Proc. IEEE Intell. Veh. Symp.*, Parma, Italy, Jun. 2004, pp. 549–554.

[28] C. R. Jung and C. R. Kelber, "Lane following and lane departure using a linear-parabolic model," *Image Vis. Comput.*, vol. 23, no. 13, pp. 1192–1202, Nov. 2005.

[29] A. Broggi, M. Cellarario, P. Lombardi, and M. Porta, "An evolutionary approach to visual sensing for vehicle navigation," *IEEE Trans. Ind. Electron.*, vol. 50, no. 1, pp. 18–29, Feb. 2003.

[30] R. Arnay, L. Acosta, M. Sigut, and J. Toledo, "Ant colony optimisation algorithm for detection and tracking of non-structured roads," *Electron. Lett.*, vol. 44, no. 12, pp. 725–727, Jun. 2008.

[31] C. F. Juang, C. M. Lu, C. Lo, and C. Y. Wang, "Ant colony optimization algorithm for fuzzy controller design and its FPGA implementation," *IEEE Trans. Ind. Electron.*, vol. 55, no. 3, pp. 1453–1462, Mar. 2008.

[32] K. Sundareswaran, K. Jayant, and T. N. Shanavas, "Inverter harmonic elimination through a colony of continuously exploring ants," *IEEE Trans. Ind. Electron.*, vol. 54, no. 5, pp. 2558–2565, Oct. 2007.

[33] C. D'Cruz and J. J. Zou, "Lane detection for driver assistance and intelligent vehicle applications," in *Proc. Int. Symp. Commun. Inf. Technol.*, Oct. 2007, pp. 1291–1296.

[34] T. Liu, N. Zheng, H. Cheng, and Z. Xing, "A novel approach of road recognition based on deformable template and genetic algorithm," in *Proc. IEEE Intell. Transp. Syst.*, Oct. 2003, pp. 1251–1256.

[35] R. Labayrade, J. Douret, J. Laneurit, and R. Chapuis, "A reliable and robust lane detection system based on the parallel use of three algorithms for driving safety assistance," *IEICE Trans. Inf. Syst.*, vol. E89-D, no. 7, pp. 2092–2100, Jul. 2006.

[36] S. Sehestedt, S. Kodagoda, A. Alempijevic, and G. Dissanayake, "Robust lane detection in urban environments," in *Proc. IEEE Intell. Robots Syst.*, Oct. 2007, pp. 123–128.

[37] C. Caraffi, S. Cattani, and P. Grisleri, "Off-road path and obstacle detection using decision networks and stereo vision," *IEEE Trans. Intell. Transp. Syst.*, vol. 8, no. 4, pp. 607–618, Dec. 2007.

[38] Q. Li, N. Zheng, and H. Cheng, "Springrobot: A prototype autonomous vehicle and its algorithms for lane detection," *IEEE Trans. Intell. Transp. Syst.*, vol. 5, no. 4, pp. 300–308, Dec. 2004.

[39] H. Y. Cheng, B. S. Jeng, P. T. Tseng, and K. C. Fan, "Lane detection with moving vehicles in the traffic scenes," *IEEE Trans. Intell. Transp. Syst.*, vol. 7, no. 4, pp. 571–582, Dec. 2006.

[40] Y. Wang, D. Shen, and E. K. Teoh, "Lane detection using spline model," *Pattern Recognit. Lett.*, vol. 21, no. 9, pp. 677–689, Jul. 2000.

[41] H. Lin, S. Ko, W. Shi, Y. Kim, and H. Kim, "Lane departure identification on highway with searching the region of interest on hough space," in *Proc. Int. Conf. Control, Autom. Syst.*, Oct. 2007, pp. 1088–1091.
[42] Y. Wang, E. Teoh, and D. Shen, "Lane detection and tracking using B-Snake," *Image Vis. Comput.*, vol. 22, no. 4, pp. 269–280, Apr. 2004.
[43] D. Heng, R. Oruganti, and D. Srinivasan, "Neural controller for UPS inverters based on B-spline network," *IEEE Trans. Ind. Electron.*, vol. 55, no. 2, pp. 899–909, Feb. 2008.
[44] Z. Lin, D. S. Reay, B. W. Williams, and X. He, "Online modeling for switched reluctance motors using B-spline neural networks," *IEEE Trans. Ind. Electron.*, vol. 54, no. 6, pp. 3317–3322, Dec. 2007.
[45] K. Szabat and T. Orlowska-Kowalska, "Performance improvement of industrial drives with mechanical elasticity using nonlinear adaptive Kalman filter," *IEEE Trans. Ind. Electron.*, vol. 55, no. 3, pp. 1075–1084, Mar. 2008.
[46] M. Chueh, Y. L. W. Au Yeung, K.-P. C. Lei, and S. S. Joshi, "Following controller for autonomous mobile robots using behavioral cues," *IEEE Trans. Ind. Electron.*, vol. 55, no. 8, pp. 3124–3132, Aug. 2008.

Bing-Fei Wu (S'89–M'92–SM'02) was born in Taipei, Taiwan, in 1959. He received the B.S. and M.S. degrees in control engineering from National Chiao Tung University (NCTU), Hsinchu, Taiwan, in 1981 and 1983, respectively, and the Ph.D. degree in electrical engineering from the University of Southern California, Los Angeles, in 1992.

From 1983 to 1984, he was with the Institute of Control Engineering, NCTU, as an Assistant Researcher. From 1985 to 1988, he was with the Department of Communication Engineering at the same university as a Lecturer. Since 1992, he has been with the Department of Electrical Engineering and Control Engineering, NCTU, where he is currently a Professor. As an active Industry Consultant, he is also involved in chip design and applications of the flash memory controller and 3C consumer electronics in multimedia. His research interests include chaotic systems, fractal signal analysis, multimedia coding, and wavelet analysis and applications.

Chuan-Tsai Lin (S'05) was born in Chunghua, Taiwan, in 1971. He received the B.S. degree in industrial education from National Chunghua University of Education (NCUE), Chunghua, in 1994, and the M.S. degree in electronic engineering from National Chung Cheng University, Chiayi, Taiwan, in 2000. He is currently working toward the Ph.D. degree in electrical and control engineering at National Chiao Tung University, Hsinchu, Taiwan.

He also teaches electronics at Changhua Senior Industrial Vocational High School, NCUE. His research interests include image processing and intelligent transportation systems.

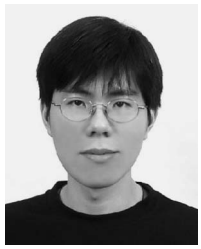

Yen-Lin Chen (S'02–M'07) was born in Kaohsiung, Taiwan, in 1978. He received the B.S. and Ph.D. degrees in electrical and control engineering from National Chiao Tung University, Hsinchu, Taiwan, in 2000 and 2006, respectively.

Since 2007, he has been an Assistant Professor with the Department of Computer Science and Information Engineering, Asia University, Taichung, Taiwan. His research interests include image and video processing, pattern recognition, document image analysis, and intelligent transportation systems.

Dr. Chen is a member of the International Association of Pattern Recognition and The Institute of Electronics, Information and Communication Engineers. In 2003, he received the Dragon Golden Paper Award sponsored by the Acer Foundation and the Silver Award of the Technology Innovation Competition sponsored by AdvanTech.